

Constraining structure formation using EDGES

Matteo Leo,^{a,b} Tom Theuns,^b Carlton M. Baugh,^b Baojiu Li^b and Silvia Pascoli^a

^aInstitute for Particle Physics Phenomenology, Department of Physics, Durham University, Durham DH1 3LE, U.K.

^bInstitute for Computational Cosmology, Department of Physics, Durham University, Durham DH1 3LE, U.K.

E-mail: matteo.leo@durham.ac.uk

Abstract. The *experiment to detect the global epoch of reionization signature* (EDGES) collaboration reported the detection of a line at 78 MHz in the sky-averaged spectrum due to neutral hydrogen (HI) 21-cm hyperfine absorption of cosmic microwave background (CMB) photons at redshift $z \sim 17$. This requires that the spin temperature of HI be coupled to the kinetic temperature of the gas at this redshift through the scattering of Lyman- α photons emitted by massive stars. To explain the experimental result, star formation needs to be sufficiently efficient at $z \sim 17$ and this can be used to constrain models in which small-scale structure formation is suppressed (DMF models), either due to dark matter free-streaming or non-standard inflationary dynamics. We combine simulations of structure formation with a simple recipe for star formation to investigate whether these models emit enough Lyman- α photons to reproduce the experimental signal for reasonable values of the star formation efficiency, f_* . We find that a thermal warm dark matter (WDM) model with mass $m_{\text{WDM}} \sim 4.3$ keV is consistent with the timing of the signal for $f_* \lesssim 2\%$. The exponential growth of structure around $z \sim 17$ in such a model naturally generates a sharp onset of the absorption. A warmer model with $m_{\text{WDM}} \sim 3$ keV requires a higher star formation efficiency, $f_* \sim 6\%$, which is a factor of few above predictions of current star formation models and observations of satellites in the Milky Way. However, uncertainties in the process of star formation at these redshifts do not allow to derive strong constraints on such models using 21-cm absorption line. The onset of the 21-cm absorption is generally faster in DMF models compared to cold dark matter (CDM) models, unless some process significantly suppresses star formation in halos with masses below $\sim 10^8 h^{-1} M_\odot$.

Contents

1	Introduction	1
2	Modeling the 21-cm signal	3
2.1	Hyperfine 21-cm absorption against the CMB	3
2.2	Structure formation	4
2.2.1	CDM models	5
2.2.2	DMF models	6
2.3	Star formation and the build-up of a Lyman- α photon background	8
3	Summary and discussion	11
A	Reionization	13

1 Introduction

Cosmic gas between us and the surface of last scattering can produce a global, redshifted ‘21-cm’ line originating from the hyperfine transition of neutral hydrogen (HI). This line appears in emission or absorption in the spectrum of the cosmic microwave background (CMB), depending on whether the spin temperature of the gas, T_s (see Section 2.1 for a definition of this quantity), is larger or smaller than the temperature of the CMB photons, T_γ . Several processes conspire to make T_s deviate from T_γ following recombination of the Universe at redshift $z \sim 1100$. Initially, Compton heating of electrons left over after recombination keeps the kinetic temperature of the gas, T_k , coupled to the temperature of the CMB, $T_k \sim T_\gamma$. Eventually, T_k decouples from T_γ below $z \sim 300$, and the gas temperature falls adiabatically as the Universe expands, $T_k \propto (1+z)^2$, whereas $T_\gamma \propto (1+z)$ [1]. Collisions between neutral hydrogen atoms keep $T_s \sim T_k$ so that $T_s < T_\gamma$, and the intervening gas appears in 21-cm absorption against the CMB. Below $z \sim 30$, the HI collision rate becomes too low to keep T_s coupled to T_k , the spin temperature increases to T_γ , and the gas becomes transparent to 21-cm photons. As the first sources of Lyman- α photons - such as *e.g.* massive stars - appear around $z \sim 20$, scattering of Lyman- α photons off HI atoms, again couple T_s to T_k through the Wouthuysen-Field (hereafter WF) effect [2, 3]. This results in $T_s \sim T_k$, and since $T_k < T_\gamma$, the cosmic gas once more appears in absorption against the CMB. The absorption signal weakens and briefly turns into emission due to heating by X-rays emitted by early black holes and/or X-ray binaries [4–6]. It is finally wiped out following reionization of the HI. For a more in-depth discussion and original references, see *e.g.* [7–12].

The EDGES¹ collaboration has reported [13] the detection of an absorption line centred at 78 MHz in the sky-averaged spectrum, which they interpret as being due to HI 21-cm absorption at $z \sim 17$ against the CMB with T_s coupled to T_k by the WF-effect. The depth of the detected absorption line corresponds to an ‘antenna temperature’ difference of $\delta T_b^{\text{min}} \sim -500$ mK, and the onset of the absorption has $\delta z \sim 3$, where δz is the redshift width from $\delta T_b = 0$ to $\delta T_b = \delta T_b^{\text{min}}$. The observed line is stronger than expected by a factor of ~ 2 . The line strength is in principle simply set by the ratio between T_k and T_γ , which are both well known in the context of the standard cosmological

¹Experiment to Detect the Global Epoch of Reionization Signature.
<https://www.haystack.mit.edu/ast/arrays/Edges/index.html>.

model (Λ CDM). The unexpected observed value may signal the need for new physical mechanisms [14] that produce an enhancement in the value of the ratio T_γ/T_k at $z \sim 17$ respect to that expected from Λ CDM calculations, for example non-gravitational dark matter (DM)-baryon interactions or the presence of extra sources of radio emission (see e.g. [15–28] for an incomplete list of references on these topics). Recently, it has been pointed out that polarized foreground contamination may produce an enhanced 21-cm absorption line [29]. More worryingly, [30] suggests that the shape - and even the reality - of the signal is potentially strongly affected by how foregrounds were modelled by [13] (but see the reply by [31]). The re-analysis of the data by [32] results in a weaker absorption signal, but the onset of the absorption remains relatively sudden. While acknowledging these concerns, the EDGES signal has been used to constrain a wide range of non-standard cosmological scenarios, see e.g. [33–39].

The shape of the downturn of the line is a measure of the rate at which stars build up a background of Lyman- α photons. In a CDM universe, the first stars form in DM halos with virial mass $M_h \sim 10^6 h^{-1} M_\odot$, when HI forms H₂ which allows the gas to cool and become self-gravitating [40]. Such ‘population three’ (Pop. III) stars are thought to form one – or at most a few – per halo, and are generically expected to be more massive than the typical star formed today because the Jeans mass in the hotter star forming gas is higher than today [41–43]. Such massive stars are hot and hence radiate copious Lyman- α photons [44]. As these stars enrich their surroundings with metals that help cool gas and promote H₂ formation, and as progressively more massive halos form, star formation is thought to become more similar to what it is today, with lower-mass ‘population two’ (Pop. II) stars forming in gas that initially cools atomically. This standard picture of the onset of star formation in the Universe results in a relatively gentle build-up of a background of Lyman- α photons, resulting in a more extended onset of the 21-cm line than observed. Reconciling the CDM model with the EDGES signal therefore requires that only halos with $M_h \gtrsim 10^8 h^{-1} M_\odot$ contribute significantly to star formation, for example because star formation in lower-mass halos is strongly suppressed due to energy injected by supernovae [45, 46].

An alternative way of making the onset of 21-cm absorption more rapid is to suppress matter fluctuations at small scales such that these lower mass halos simply do not form, by changing either the nature of the DM or the physics of the very-early universe. If the DM has a large free-streaming length, it smooths out small-scale structure below some characteristic damping scale λ_d , because of the intrinsic velocities of the DM particles [47–60]. Such models are generically termed ‘warm dark matter’ (WDM) models². Small-scale power can also be suppressed due to non-standard inflationary dynamics [67–71]. We will refer to a model in which power is significantly suppressed below some scale λ_d (compared to CDM) generically as a model with damped matter fluctuations (DMF), and the co-moving mass in a volume with radius λ_d as the ‘damping mass’, M_d . The onset of *star* formation may be very different in DMF models, because the first structures to collapse are extended filaments with a mass of order of the damping mass, rather than halos [72] (see also [73]). The very different nature of the DM potential wells in which the first stars form is likely to affect the nature of these stars - for example their mass - as well as the abundance of such stars - *i.e.* the total number of stars formed per unit volume. Making accurate *quantitative* predictions for how this affects the 21-cm signal is challenging. However, generically we expect these stars to form more abundantly and be of higher mass compared to CDM models, mainly because the filaments can collect a large amount of gas *before* any stellar processes can limit gas accretion. The latter is because there is no stellar feedback in progenitors as a result of the progenitor halos themselves not forming (see [72] for more

²In the context of alternative DM scenarios, a suppression of the gravitational clustering on small scales can be also achieved allowing DM particles to have non-vanishing interactions (either with themselves [61] or with neutrinos/photons [62, 63]) or considering models where DM is a scalar field with a macroscopic wave-like behaviour [64–66].

details along these lines). We therefore expect any 21-cm signal to build up rapidly.

Independent motivation for examining DMF models comes from particle physics. For example, sterile neutrinos act as WDM and have been proposed to explain the observed baryon asymmetry of the Universe ([74], see [75] for a recent review). In addition, WDM has been proposed as a solution to some perceived astrophysical problems related to the number density and concentration of dwarf galaxies [47–49] (see [76] for a recent review). Constraints on the ‘warmness’, *i.e.* the scale λ_d below which WDM suppresses structure, is often quoted in terms of the mass, m_{WDM} , of the thermal WDM particle with the same value of λ_d . Observations of the Lyman- α forest [50, 77–80] and constraints resulting from the observed satellite luminosity function of the Milky Way galaxy [81, 82] robustly exclude thermal WDM candidates with masses lower than $m_{\text{WDM}} \sim 2$ keV. Indeed, in these models *less* structure forms than observed.

The timing of the EDGES signal constrains λ_d : too much suppression delays structure formation and hence the Lyman- α background also builds up too late [27, 83–87]. Here we re-examine this constraint. This paper is structured as follows. We begin with a brief overview of how the emission of Lyman- α from young galaxies is related to the 21-cm signal through the WF-effect in Section 2.1. The DM models that we use are introduced in Section 2.2, together with details of the numerical simulations for calculating the rate of formation of DM structures in which the young galaxies form. The 21-cm signal corresponding to the different models is discussed in Section 2.3. Finally, Section 3 summarizes our findings.

2 Modeling the 21-cm signal

2.1 Hyperfine 21-cm absorption against the CMB

This section briefly reviews the well-known physics behind 21-cm HI hyperfine absorption against the CMB see *e.g.* [10]. The strength of the absorption depends on three temperatures, (i) the spin temperature, T_s , (ii) the kinetic temperature of the gas, T_k , and (iii) the CMB temperature, T_γ . When HI atoms are in the electronic ground state, T_s sets the fraction of atoms that are in the higher energy triplet state (proton and electron have parallel spin, state n_1) compared to the singlet state (anti-parallel spins, state n_0),

$$\frac{n_1}{n_0} = \frac{g_1}{g_0} \exp\left(-\frac{T_\star}{T_s}\right). \quad (2.1)$$

Here, T_\star is the atomic constant $T_\star \equiv hc/(k_B \lambda_{21}) \approx 0.068$ K, with h Planck’s constant, k_B Boltzmann’s constant, c the speed of light, and $\lambda_{21} \approx 21.1$ cm the wavelength of the 21-cm line; $g_1/g_0 = 3$ is the ratio of degeneracy levels of the triplet to the singlet state. In equilibrium, $T_s = T_k = T_\gamma$, and neutral gas absorbs 21-cm photons from the CMB at the same rate that it emits such photons making the gas transparent. When $T_s < T_\gamma$, more photons are absorbed than emitted, and intervening gas appears in absorption against the CMB. The intensity of the absorption signal strength depends on T_s .

It is customary in radio astronomy to quantify the specific intensity of a signal at frequency ν , I_ν , in terms of its ‘apparent brightness’ or ‘antenna temperature’. This is the temperature of a black body that has the same value of I_ν in the Rayleigh-Jeans part of the spectrum, $I_\nu = 2k_B T \nu^2 / c^2$. The strength of the 21-cm absorption is then the temperature difference, δT_b , between the brightness temperature of the signal and that of the CMB. It is related to T_s by (as given in [10]),

$$\delta T_b \approx 27 \text{ mK } x_{\text{HI}}(z) \left(\frac{\Omega_b h^2}{0.023} \right) \left(\frac{0.15}{\Omega_m h^2} \frac{1+z}{10} \right)^{1/2} \left(1 - \frac{T_\gamma(z)}{T_s(z)} \right). \quad (2.2)$$

Here, $x_{\text{HI}}(z) \approx 1$ at $z \sim 17$ is the fraction of gas in the form of HI (see *e.g.* [8]), $T_\gamma = T_\gamma^0(1+z)$ is the CMB temperature in terms of its value $T_\gamma^0 \approx 2.73$ K today; Ω_b and Ω_m are the cosmological baryon density and total matter density in units of the critical density, respectively. $\delta T_b < 0$ occurs for $T_s < T_\gamma$, which signals absorption.

The situation where $T_s < T_\gamma$ arises when T_s gets coupled to T_k , because as the Universe cools adiabatically, T_k drops faster than T_γ , so that $T_s \approx T_k$ results in $T_s < T_\gamma$. Such coupling can be caused by collisions in sufficiently dense regions and by scattering of Lyman- α photons produced by early sources such as hot stars through the WF-effect. The basic physics behind the WF-effect is that when an HI atom in the $n = 1$ electronic ground state absorbs and then re-emits a Lyman- α photon, it can flip from the singlet to the triplet state or vice-versa. However, when $T_s = T_k$, then there should be no net energy transfer between the hyperfine states and the gas, therefore Lyman- α scattering will couple T_s to T_k . The coupling strength depends on atomic constants and the specific mean intensity J_α of the radiation at the Lyman- α wavelength (*e.g.* [88–90]),

$$\begin{aligned} 1 - \frac{T_\gamma}{T_s} &= \frac{x_\alpha}{1 + x_\alpha} \left(1 - \frac{T_\gamma}{T_k} \right) \\ x_\alpha &= \frac{16\pi^2 T_* e^2 f_\alpha}{27 A_{10} T_\gamma m_e c} S_\alpha J_\alpha. \end{aligned} \quad (2.3)$$

Here, $f_\alpha = 0.4162$ is the oscillator strength of the Lyman- α line, $A_{10} = 2.85 \times 10^{-15} \text{ s}^{-1}$ is the Einstein coefficient of the 21-cm transition, e and m_e are the electron charge and mass, respectively; S_α is a correction factor that accounts for spectral distortions for which we take $S_\alpha \simeq 1$ following [90]. The required Lyman-alpha flux needed for effective WF coupling was estimated *e.g.* in [91].

If the HI atom had only two electronic energy levels, then J_α would simply be the background of Lyman- α photons produced by early sources. However, Lyman- α photons can be produced by the absorption of photons in the higher Lyman series, followed by a radiative cascade. We also need to account for photons redshifting out of, and into, the Lyman- α transition. Taking all of this into account relates J_α to the emissivity of the sources, $\epsilon_\nu(z)$, as [88–90]

$$J_\alpha(z) = \frac{c(1+z)^2}{4\pi} \sum_{n=2}^{23} f_n \int_z^{z_{\text{max},n}} dz' \frac{\epsilon_\nu(z')}{H(z')}. \quad (2.4)$$

Here, the f_n are atomic constants related to the radiative cascade (see *e.g.* [90] for the numerical values of f_n), $H(z)$ is the Hubble constant, and $z_{\text{max},n}$ is given by [10] as

$$z_{\text{max},n} = (1+z) \left(\frac{1 - (1+n)^{-2}}{1 - n^{-2}} \right) - 1. \quad (2.5)$$

We will assume that the sources of UV-photons are hot stars that form in collapsed structures. Therefore to compute $\epsilon_\nu(z)$, we first need to know the fraction of mass that collapses into bound structures in which star formation can proceed, $f_{\text{coll}}(z)$. This fraction depends on cosmology and on the shape of the power spectrum, as we examine next.

2.2 Structure formation

We want to contrast the expected 21-cm signal in CDM models to that in alternative models in which the power below some co-moving damping scale λ_d is suppressed compared to CDM. We begin by describing how we calculate $f_{\text{coll}}(z)$ in CDM models.

2.2.1 CDM models

To compute f_{coll} , we start by computing the evolution of the halo mass function, $n(M, z)$, for which we use the Sheth-Tormen (ST) extension [92] of the Press-Schechter (PS) formalism [93–96]. The halo mass function is the (co-moving) number density of halos of mass M at redshift z , and is given by

$$\frac{dn_{\text{CDM}}}{d\ln(M)} = \frac{1}{2} \frac{\bar{\rho}_m^0}{M} f(\nu) \frac{d\ln(\nu)}{d\ln(M)}, \quad (2.6)$$

where $\bar{\rho}_m^0$ is the mean co-moving matter density and

$$\nu = \frac{\delta_{c,0}^2}{\sigma^2(R)D^2(z)}. \quad (2.7)$$

Here, $\delta_{c,0} = 1.686$, $D(z)$ is the linear growth factor normalized to $D = 1$ at $z = 0$, and $\sigma^2(R)$ is the mass-variance on scale R ,

$$\sigma^2(R) = \int \frac{d^3\mathbf{k}}{(2\pi)^3} P_{\text{CDM}}(k) \tilde{W}^2(k|R). \quad (2.8)$$

In this expression, $P_{\text{CDM}}(k)$ is the linear matter power spectrum at $z = 0$ and $\tilde{W}(k|R)$ is (the Fourier transform of) the filter function. We use a spherical top-hat (other window functions have been discussed in the literature, see *e.g.* [94, 96–99]), given in real space by

$$W(r|R) = \begin{cases} \frac{3}{4\pi R^3} & \text{if } r \leq R \\ 0 & \text{if } r > R \end{cases}. \quad (2.9)$$

The ST formalism uses the ellipsoidal collapse model of [92] to compute $f(\nu)$. This function is well approximated by

$$f(\nu) = A \sqrt{\frac{2q\nu}{\pi}} \left(1 + (q\nu)^{-p}\right) \exp(-q\nu/2), \quad (2.10)$$

with $A = 0.3222$, $p = 0.3$ and $q = 0.707$.

The damping mass M_d is effectively zero in CDM and consequently all dark matter is in collapsed objects of some mass at any z , $f_{\text{coll}} \approx 1$. However, the numerous low-mass dark matter halos that form at high z will not contribute significantly to star formation and hence are irrelevant for computing ϵ_ν . The reason is that, if the virial temperature, T_{vir} , of a halo is too low, the gas is too cold to cool and form stars. For $T_{\text{vir}} \sim 8000$ K, the gas is thought to be hot enough to cool via the formation of H_2 [40], once $T_{\text{vir}} \sim 10^4$ K, gas can cool by atomic transitions in HI (see *e.g.* [7] for more details). To account for this, we will only include DM halos above a given minimum mass³ when computing the collapsed fraction f_{coll} . Below we will illustrate CDM results for $M_{\text{min}} = 10^7 h^{-1} M_\odot$ and $M_{\text{min}} = 10^8 h^{-1} M_\odot$, denoting these models by ‘CDM-7’, and ‘CDM-8’ respectively. Given $n(M, z)$, we can compute the collapsed fraction for these models as

$$f_{\text{coll}}(z) = \frac{1}{\bar{\rho}_m^0} \int_{M_{\text{min}}}^{\infty} dM M \frac{dn_{\text{CDM}}(z)}{dM}. \quad (2.11)$$

³A given minimum halo mass can be converted to a corresponding minimum virial temperature of the star forming halo using Eq. (26) in [7].

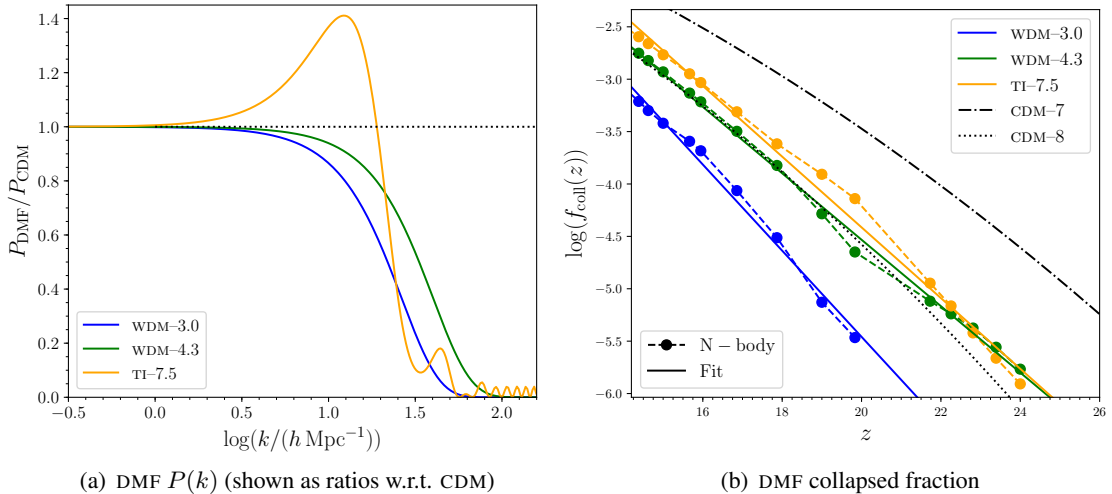


Figure 1. (a) Ratios w.r.t. CDM of the linear theory power spectra for WDM and TI models (as labelled). (b) Evolution of the collapsed fraction, $f_{\text{coll}}(z)$, for the three DMF (colour) and the two CDM (black) models considered in this analysis. In the case of DMF, symbols show the results from the simulation, while solid lines show those from the parametrisation Eq. (2.14), with parameters reported in Table 1. The $f_{\text{coll}}(z)$ for CDM are obtained from the Sheth-Tormen extension of the Press-Schechter formalism (see main text for more details).

Model	WDM-3.0	WDM-4.3	TI-7.5
f_{14}	1.02×10^{-3}	2.34×10^{-3}	4.08×10^{-3}
ζ	0.95	0.73	0.78

Table 1. Fitting parameters f_{14} and ζ for the fit of Eq. (2.14) to the evolution of the fraction of mass in collapsed objects plotted in Fig. 1(b), for the three DMF models, WDM-3.0, WDM-4.3 and TI-7.5.

The evolution of f_{coll} in the range of redshifts considered in our analysis is shown in Figure 1(b) for CDM-7 and CDM-8. As expected, the values of the collapsed fraction are always larger in CDM-7 than CDM-8 because more halos are included in the calculation of the former. An interesting difference between the two CDM models is that the build-up of structure in CDM-8 is more rapid than in CDM-7. We will return on this aspect when discussing the results in Section 2.3.

2.2.2 DMF models

For the WDM models, we introduce an exponential cut-off in the power spectrum to mimic the effect of free-streaming,

$$P_{\text{WDM}}(k) = P_{\text{CDM}}(k) \exp(-\lambda_d^2 k^2). \quad (2.12)$$

We examine two models, taking $\lambda_d = 0.038 h^{-1} \text{ Mpc}$ and $\lambda_d = 0.025 h^{-1} \text{ Mpc}$, which correspond to two choices for the WDM thermal-equivalent particle mass⁴ $m_{\text{WDM}} \sim 3 \text{ keV}$ and $m_{\text{WDM}} \sim 4.3 \text{ keV}$. We will refer to these models as WDM-3.0 and WDM-4.3, respectively. Note that our Eq. (2.12) is considered as an approximation of the real effect of the free-streaming on the linear matter power spectrum of WDM models. Power spectra that are more accurate than simply imposing an exponential cut-off can be generated using either Boltzmann codes such as CLASS [100, 101] or the transfer function proposed in [47, 50]. The advantage of adopting an exponential cut-off resides in the fact that, the only free-parameter in the exponential (λ_d , see Eq. (2.12)) unequivocally identifies the scale

⁴More accurately, the two mass values are $m_{\text{WDM}} = 2.92 \text{ keV}$ and $m_{\text{WDM}} = 4.25 \text{ keV}$.

of the damping. On the other hand, transfer functions as that in [47, 50] depend on the particular WDM model considered and are, in general, given in terms of particle physics parameters (such as the mass of the WDM candidate), whose relation with the damping scale is more subtle than that displayed in Eq. (2.12). Nevertheless, we expect that our results on the 21-cm absorption signal will not change dramatically when considering more accurate power spectra than those employed here. We additionally consider a thermal inflation (TI) model with $k_b = 7.5 \text{ Mpc}^{-1}$ (k_b represents the wave number above which the TI linear power spectrum starts to deviate appreciably from that of standard CDM, see [68]), generated using the transfer function calculated by [68, 69],

$$T_{\text{TI}}(\xi) = \cos \left[\xi \int_0^\infty \frac{d\alpha}{\sqrt{\alpha(2 + \alpha^3)}} \right] + 6\xi \int_0^\infty \frac{d\gamma}{\gamma^3} \int_0^\infty d\beta \left(\frac{\beta}{2 + \beta^3} \right)^{3/2} \sin \left[\xi \int_\gamma^\infty \frac{d\alpha}{\sqrt{\alpha(2 + \alpha^3)}} \right], \quad (2.13)$$

where $\xi = k/k_b$ and the power spectrum is $P_{\text{TI}}(k) = P_{\text{CDM}}(k)T_{\text{TI}}^2(k)$; we will refer to this model as TI-7.5. The suppression of power compared to CDM is plotted in Figure 1(a) for these three models. For the WDM models, we see that a larger value of m_{WDM} suppresses power on smaller scales (*green* versus *blue* curve). The power-spectrum of the TI-7.5 model (*yellow* curve) is suppressed more strongly than WDM-4.3 for $k \gtrsim 25 h \text{ Mpc}^{-1}$, however at wave numbers in the range $k \in [5, 20] h \text{ Mpc}^{-1}$, the power in TI-7.5 is *enhanced* compared to CDM. This characteristic enhancement is one of the main features of this model, compared to WDM. Its impact on the non-linear power spectrum and halo abundances has been studied by [70]; the effects on structure formation of other models with two inflationary stages have also been investigated by [71].

Given these linear power spectra, we have performed DM only cosmological simulations of structure formation, using the tree-PM N-body code Gadget-2 [102]. Initial conditions were generated at $z = 199$, an epoch in which all the wave numbers probed in the simulation are well inside the linear regime, using second-order Lagrangian perturbation theory with 2LPTic [103]. We choose a box of co-moving length $L_{\text{box}} = 5 h^{-1} \text{ Mpc}$ and employ $N_{\text{box}} = 1024^3$ simulation particles⁵. The three models are evolved up to $z = 14$, using a Plummer-equivalent gravitational softening length that is kept constant at 1/40-th of the mean interparticle spacing. In the redshift ranges considered in our analysis, the k -modes with largest amplitudes just enter the non-linear regime by $z \approx 14$.

We identify collapsed structures using a friend-of-friends (FoF) algorithm with a linking length of $b = 0.2$ times the mean interparticle spacing. We only consider FoF structures with more than 10^3 particles, corresponding to a mass $M_{\text{DM}} > M_{\text{threshold}} \sim 10^7 h^{-1} M_\odot$. Such structures are numerically well resolved and the simulations also resolve halo masses near the damping mass M_d even in the coldest WDM model. In addition, any *lower mass* objects have a virial temperature below $T \sim 10^4 \text{ K}$ that is too low to enable cooling by HI [7]. Gas in lower mass halos, if they were to form, would only cool through H_2 formation, but this channel is suppressed in DMF models (see discussion in [87]). We sum all of the mass in collapsed structures to compute $f_{\text{coll}}(z)$, the fraction of mass that is in collapsed objects. Note that the choice of the linking length to identify collapsed structures in simulations is somewhat uncertain (see *e.g.* [104] for the case of WDM simulations). Understanding the full impact of different choices of b on the fraction of collapsed objects at $z \sim 17$ is beyond the scope of this paper. However, in the next subsection, when acknowledging the possible uncertainties in our method for estimating the 21-cm absorption signal, we will briefly describe the expected overall effect of varying b on f_{coll} .

⁵The simulation particle mass is $m_{\text{sim}} \simeq 1.01 \times 10^4 h^{-1} M_\odot$.

Model	WDM-3.0	WDM-4.3	TI-7.5	CDM-7	CDM-8
f_*	0.061	0.017	0.011	0.003	0.017

Table 2. Values of f_* obtained by imposing $x_\alpha = 1$ at $z = 17.2$ as described in Section 2.3.

The evolution of f_{coll} in DMF models can be understood by considering the evolution of the halo mass function, $n(M, z)$, discussed in the previous section in the context of the PS approach. In the PS model, $n(M, z)$ is a power-law at $M < M_{\text{ST}}(z)$, and exhibits an exponential cut-off at $M > M_{\text{ST}}(z)$. Here, $M_{\text{ST}}(z)$ is a characteristic mass which increases with time. At sufficiently high z , $M > M_{\text{ST}}(z)$, and $n(M, z)$ is exponentially small. As time increases, so does M_{ST} , until eventually $M \approx M_{\text{ST}}$, causing the abundance of structure of mass M , $n(M, z)$, to increase exponentially. Eventually, $M \ll M_{\text{ST}}$, $n(M, z)$ remains on the power-law tail of the PS mass function and $n(M, z)$ evolves slowly. We can estimate the value of $M_{\text{ST}}(z)$ when objects start to form in our DMF model, as follows. Setting $M_{\text{ST}}(z = 0) \sim 10^{14} h^{-1} M_\odot$ and taking the approximate growth rate $M_h(z) = M_h(z = 0)(1 + z)^{0.24} \exp(-3z/4)$ from [105], yields $M_{\text{ST}}(z = 20) \approx 10^8 h^{-1} M_\odot$, consistent with the numerical results of [106]. Applying this reasoning to the special case of DMF models, we infer that very little structure forms before M_{ST} , which is set by cosmology, becomes of order of the damping mass M_d , which is set by λ_d . As soon as these masses become comparable, structures will emerge and f_{coll} will increase exponentially. When M_{ST} becomes much larger than M_d , the rate of increase of f_{coll} will decline. This expectation is borne-out by the simulations. In Figure 1(b), we plot the total mass in collapsed objects in our $L_{\text{box}} = 5 h^{-1} \text{Mpc}$ simulations, for the three DMF models. Coloured straight-lines are fits of the form

$$f_{\text{coll}}(z) = f_{14} \exp(-\zeta(z - 14)), \quad (2.14)$$

to the simulation results, with parameters f_{14} and ζ reported in Table 1. The fits reproduce the simulation results well, and we use them to compute the evolution of f_{coll} in the DMF models⁶.

We now have expressions for the fraction of mass in collapsed objects in which we assume that stars form, both in CDM and in DMF models. Next we describe how we use f_{coll} to describe the onset of star formation and the build-up of a Lyman- α background.

2.3 Star formation and the build-up of a Lyman- α photon background

We characterize the star formation efficiency of collapsed structures by the parameter f_* , which relates the (co-moving) star formation rate density, $\dot{\rho}_*$, to the rate at which structures collapse,

$$\dot{\rho}_*(z) = f_* \bar{\rho}_b^0 \frac{df_{\text{coll}}(z)}{dt}, \quad (2.15)$$

where $\bar{\rho}_b^0$ is the present day baryon density. For a single galaxy in a halo, f_* sets the ratio of the stellar mass to halo mass,

$$f_* = \frac{M_*/\Omega_b}{M_h/\Omega_m}. \quad (2.16)$$

This expression allows us to estimate a maximal value for f_* . Ref. [107] presents a model of feedback-regulated galaxy formation, in which the star formation rate of a galaxy is set by the balance between the energy lost by the deepening of the potential of its host dark matter halo due to cosmological accretion and the energy injected by supernovae. The model predicts a ratio $M_*/M_h \sim 10^{-3}$

⁶We expect that the exponential accretion of the collapsed fraction (Eq. (2.14)) in DMF will be replaced by a power-law evolution at later redshifts ($z < 14$), similar to what found in [105] for CDM.

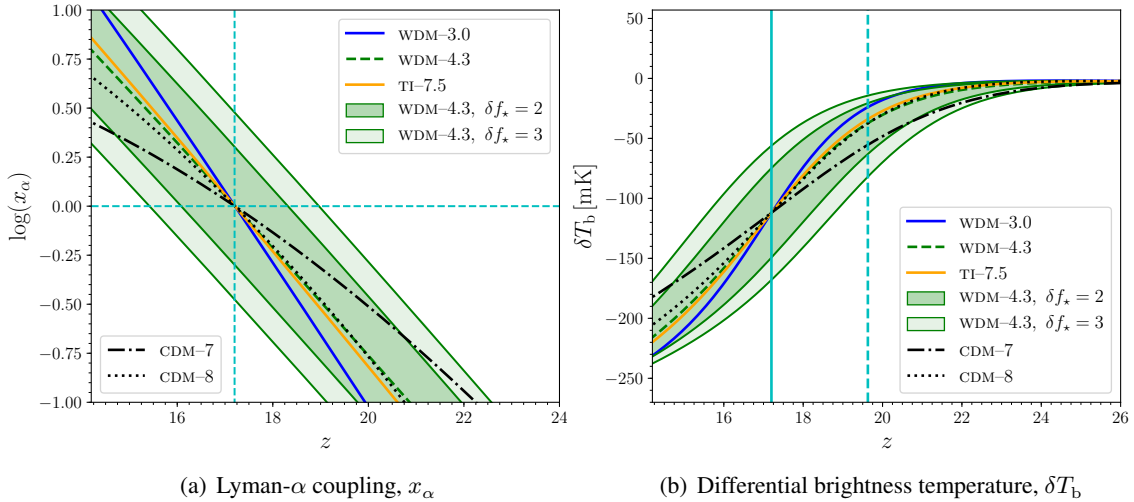


Figure 2. (a) Lyman- α coupling constant x_α for the five models considered here (different colour lines show different models as labelled), calculated imposing $x_\alpha = 1$ at $z = 17.2$, shown in the figure as intercept of the two cyan dashed lines. The colored bands show the values in the range $[x_\alpha/\delta f_\star, x_\alpha \times \delta f_\star]$ for $\delta f_\star = 2$ (dark green shaded area) and $\delta f_\star = 3$ (light green shaded area). (b) Evolution of the differential brightness temperature δT_b as a function of the redshift z for the different models, calculated from the x_α values in Figure 2(a). The cyan vertical solid line shows the redshift corresponding to the mean frequency of the EDGES experiment, while the cyan vertical dashed line represents the redshift where the amplitude of the EDGES signal is at half of its maximum (these are the same as those shown in [83]). Note that we do not attempt to model the X-ray background heating of the hydrogen gas, which makes the signal disappear at late times.

for a halo of mass $M_h = 10^8 M_\odot$ at $z \sim 17$, corresponding to $f_\star = 0.5\%$. The cosmological hydrodynamical simulation presented by [108] give a similar median ratio of M_\star/M_h in $M_h \sim 10^8 M_\odot$ halos, but with a relatively large scatter. Observations of satellites in the Milky Way also give a similar value for the stellar fraction at this halo mass (see [108], their Fig. 4). We will consider a model to be viable provided $f_\star \in [0.1, 2]\%$, that is within a factor of 4 larger or smaller than our best estimate.

We further assume that the co-moving UV-emissivity, $\epsilon_\nu(z)$, is proportional to the star formation rate,

$$\epsilon_\nu(z) = \epsilon_b(\nu) \frac{\dot{\rho}_\star(z)}{m_H}, \quad (2.17)$$

where m_H is the proton mass. Here, $\epsilon_b(\nu)$ is the number of photons per unit of frequency emitted at frequency ν per baryon in stars. We assume that $\epsilon_b(\nu)$ is constant over the interval $[\nu_\alpha, \nu_L]$ (where ν_L is the Lyman-limit frequency). We choose $\epsilon_b(\nu)$ so that a given number, N_α , of photons is produced per baryon in stars in the frequency interval $[\nu_\alpha, \nu_L]$. If Pop. II stars are the dominant sources of UV photons, then $N_\alpha \approx 9690$ [88], using the STARBURST99 model by [109]. Given $f_{\text{coll}}(z)$, as computed in the previous section, these two equations yield $\epsilon_\nu(z)$, which allows the calculation of the specific mean intensity of Lyman- α photons, $J_\alpha(z)$, using Eq. (2.4).

The calculation presented so far involves several uncertain parameters. The first parameter is our choice of linking length, b , used to identify collapsed structure in the DMF simulations. Secondly, the star formation efficiency, f_\star , is not very well known. Previously we argued that we expect that a reasonable model should have $f_\star \in [0.1, 2]\%$ (in halos of mass $M_h \sim 10^8 M_\odot$), but in fact f_\star is likely to depend on halo mass (see *e.g.* [110–112] for detailed studies on the dependence of f_\star on halo mass and redshift). Once stars start to form in a galaxy, supernovae associated with the end-stages of massive stars inject a large amount of energy into the galaxy, and this may strongly suppress further

star formation, see *e.g.* [113]. The importance of this feedback loop will depend on the nature of the galaxy – in particular on the depth of its gravitational potential – as well as on the nature of the stars. In addition, the minimum halo mass in which star formation will occur is not well known, as briefly discussed in the previous section. Finally, the function $\epsilon_b(\nu)$ that relates $\dot{\rho}_*$ to ϵ_ν depends on the nature of the stars – in particular on the initial stellar mass function – which is not very well known.

To make progress, we proceed as follows. The exponential build-up of mass in DMF models means that ϵ_ν is mostly determined by the star formation efficiency of halos with mass around the damping mass, M_d , given our choice of models. The value of f_{coll} in such halos depends on the linking length b - but a different choice of b will simply result in a larger or smaller value of f_{coll} without affecting its evolution. As a consequence, the uncertainty in parameters - b , f_* and ϵ_ν - will simply appear as an overall normalization constant in the value of $J_\alpha(z)$. Of course, the value of this normalization constant is of interest, yet our modelling is sufficiently uncertain that we cannot hope to calculate it with any real accuracy. Therefore, we instead *choose* f_* in each of our DMF models such that the Lyman- α coupling coefficient from Eq. (2.3) is unity at $z = 17.2$ (the redshift corresponding to the mean frequency of the EDGES experimental absorption signal [13]), *i.e.* $x_\alpha(z = 17.2) = 1$. We choose this value because it gives a 21-cm absorption signal that is in relatively good agreement with the *timing* of the EDGES detection. The required value for f_* for all DMF models is specified in Table 2, given the evolution of f_{coll} and choice of linking length $b = 0.2$ discussed in the previous section, and taking $N_\alpha = 9690$. Given that we demand that a reasonable model should have f_* in the range of 0.1–2%, the *timing* of the EDGES signal seems to disfavour the WDM-3.0 model. In this model, structure formation is so much suppressed that the structures that do form need to be much more efficient in forming stars than what is currently thought reasonable.

Assuming that f_* is a constant is less well motivated for the CDM case. Indeed, a relatively extended range of halo masses can in principle contribute to the build-up of J_α , and it is quite unlikely that star formation is equally efficient in all these halos (see *e.g.* [110–112]). The values for f_* that yield $x_\alpha(z = 17.2) = 1$ for the two CDM case with different choices for M_{min} , are also given in Table 2 (assuming our default value of $N_\alpha = 9690$). Both models require reasonable values of f_* .

The two key quantities x_α and δT_b describing the 21-cm absorption feature are computed using the Accelerated Reionization Era Simulations code (ARES) [111, 114–116]. We provide the code with the star formation rate density, Eq. (2.15). Note that we do not attempt to model the upturn of the absorption signal at lower redshifts, so we consider the background X-ray efficiency parameter and the ionizing photon efficiency parameter to be $f_X = 0$ and $f_{\text{esc}} N_{\text{ion}} = 0$, respectively (see [115] for a definition of f_X , while f_{esc} , N_{ion} are introduced in Appendix A).

The resulting evolution of the Lyman- α coupling constant, $x_\alpha(z)$, is plotted in Fig. 2(a) for all five models; CDM models are shown in *black*, DMF models in *colour*. We note that $x_\alpha(z = 17.2) = 1$ for all models, by construction; *cyan dashed lines* are drawn at $z = 17.2$ and $x_\alpha = 1$, to guide the eye. The effect of increasing or decreasing f_* by a factor 2 and 3 for model WDM-4.3, are shown by *dark* and *light green* shading, respectively. In all DMF models, x_α increases exponentially with time, reflecting the exponential increase in the collapsed fraction. Once scaled to have $x_\alpha(z = 17.2) = 1$, there is little difference between them. The CDM-8 model, which has $M_{\text{min}} = 10^8 h^{-1} M_\odot$ (*dotted black line*) looks very similar to the DMF models. This is not surprising since we neglect any halos below M_{min} in the calculation of f_{coll} - effectively making the CDM model behave like a DMF model with $M_d \sim M_{\text{min}}$ (f_{coll} in CDM-8 is very similar to that in other DMF models, especially WDM-4.3, see Figure 1(b)). In all these models, x_α increases rapidly with time, from $\log(x_\alpha) = -0.5$ to $+0.5$ over a redshift extent $\Delta z \approx 3$. The build-up of x_α in the CDM-7 model, which has $M_{\text{min}} = 10^7 h^{-1} M_\odot$ (*dashed black line*), is considerably more extended in redshift, requiring $\Delta z \gtrsim 5$ for a ten-fold increase in x_α . This is a direct result of lower-mass halos, whose abundance does not increase rapidly

in time, contributing significantly to J_α .

The corresponding evolution of the brightness temperature difference, δT_b , is shown in Fig. 2(b), using the same colour/line style conventions. The *cyan vertical solid line* at $z = 17.2$ is the mean redshift of the EDGES signal, while the *cyan vertical dashed line* represents the redshift where the amplitude is at half of its maximum. They are drawn to roughly indicate the range of redshifts spanned by the absorption trough of the EDGES signal in its downturn region. Note that all the models in Fig. 2(b) predict $\delta T_b \simeq -112$ mK at $z = 17.2$, which is expected because we have scaled f_\star to yield $x_\alpha = 1$ at $z = 17.2$ for all the models. As could be expected from the earlier discussion, the onset of 21-cm absorption is more rapid in the DMF and CDM-8 models, compared to the CDM-7 model. However, deciding which, if any, of these look like the EDGES detection is not obvious. In particular, since we do not attempt to model the *decrease* of the absorption at lower z , thought to be caused by X-ray heating, we cannot compare the mean redshift of the simulated absorption line to the EDGES data. Moreover, the absorption line is much stronger in the data than can be understood by simply coupling T_s to T_k through the WF-effect, as discussed in the Introduction. According to [83], $\delta T_b^{\min} \in [-180, -100]$ mK before the upturn caused by X-ray heating, and models are allowed if the position of the minimum (δT_b^{\min}) appears at $z \gtrsim 17.2$. Since all our models predict the same value of $\delta T_b \in [-180, -100]$ mK at $z = 17.2$, they are all allowed based on the [83] criterion.

However, from a comparison between our results in Figure 2(b) and the downturn of the EDGES signal, we can conclude that the results for the DMF and CDM-8 models are overall in better agreement with the range of redshifts spanned by the observed absorption trough than those of the CDM-7 model. Indeed, in the case of CDM-7, the downturn of the brightness temperature starts at higher redshifts and its profile is considerably shallower. Note that the situation is even worse for CDM had we allowed star formation with the same efficiency in halos with mass lower than $10^7 h^{-1} M_\odot$, *e.g.* by invoking significant star formation through molecular cooling of gas. The impact of such ‘Pop. III’ star formation in CDM is uncertain, because the build-up of a background of Lyman-Werner radiation by this mode of star formation leads to strong negative feedback, limiting the number of Pop III stars that can form, see *e.g.* [117].

We conclude noticing that pre-recombination differential streaming of baryons with respect to dark matter [118] may affect the formation of the first stars and galaxies. However, these effects are thought to be small for halos of mass larger than $10^7 h^{-1} M_\odot$, see *e.g.* [119, 120], and hence would not affect our conclusions.

3 Summary and discussion

The 21-cm signal in the pre-reionization era can be used to constrain models with damped matter fluctuations on small scales, because these models introduce a scale below which there is a delay of structure formation with respect to CDM models. Deriving constraints using 21-cm physics in a given cosmological model requires knowledge of several ingredients: (i) the evolution of the fraction of dark matter in collapsed structures that can form stars, f_{coll} , (ii) the star formation efficiency of these halos, f_\star , and (iii) the rate at which stars produce Lyman- α photons, for example quantified in terms of the number of Lyman- α photons emitted per baryon in stars, N_α . The signal shape also depends on the rate at which the gas is heated by X-rays, a process that we have not modelled. As stressed by [87], all three of these ingredients are relatively poorly understood and introduce uncertainties into the calculation of the global 21-cm signal. In particular it is not even clear whether the emergence of the first star forming galaxies in DMF models resembles that in CDM: there are good reasons to suspect the existence of significant differences [72, 73].

In [87], the authors have shown that the constraints from [83] on the scale M_d below which structure formation is depressed in DMF models, can be loosened if a higher star formation efficiency parameter is chosen. However, in all these previous works, the value of f_* has been held fixed for all models. Here, we have taken a different approach, namely picking f_* for each model such that it reproduces the timing of the 21-cm line, and contrasting the rate at which the 21-cm signal builds up. This aspect of the modelling is particularly relevant in terms of the *shape* of the signal. Our findings can be summarized as follows:

- Warm dark matter models with thermal-equivalent particle mass $m_{\text{WDM}} \sim 3 \text{ keV}$ can produce an absorption signal in line with the timing of the EDGES results but only if $f_* \sim 6\%$. We argued that such a star formation efficiency is higher than values coming from predictions of current star formation models and observations of satellites in the Milky Way, disavouring this model. The colder model with $m_{\text{WDM}} > 4 \text{ keV}$ requires $f_* \lesssim 2\%$. Our model of thermal inflation, TI-7.5, requires $f_* \sim 1.1\%$. Given the uncertainties in the modelling, we argue that both these models are consistent with the timing of the EDGES signal.
- A CDM model in which star formation in halos below a mass of $M_{\text{min}} = 10^8 h^{-1} M_\odot$ is assumed to be negligible, for example due to stellar feedback, requires $f_* \sim 1.7\%$, and is almost indistinguishable from our DMF models. From the point of view of the 21-cm physics, it will be hard to distinguish such a CDM model from a DMF model.
- Reducing the minimum mass for a halo to undergo star formation to $M_{\text{min}} = 10^7 h^{-1} M_\odot$ in CDM does lead to generic differences with DMF models. In such a model, a larger fraction of Lyman- α photons is produced by stars that form in low-mass halos. The number density of such halos increases only slowly with time around $z \sim 17$, and this results in a more extended onset of the 21-cm absorption signal. Moreover, the value of f_* required in such a model is only $f_* = 0.3\%$. If f_* were to remain constant, which is in fact unlikely, than such a low star formation efficiency results in reionization below $z \sim 5$ (the result is shown in the Appendix). Reducing the minimum mass to even lower values than $10^7 h^{-1} M_\odot$ would strengthen the above conclusion.
- Taken at face value, none of our models results in an onset of the 21-cm signal that is as rapid as the observed EDGES signal (c.f. Figure 2(b)). However, the more that low-mass halos contribute to Lyman- α photon production, the shallower the resulting onset. Therefore we find that DMF models, if anything, are *preferred* by the EDGES signal, rather than ruled out. CDM models can still produce a rapid onset of 21-cm absorption, but only if the physics of star formation conspires with that of structure formation, to make the CDM model mimic the DMF model. An example is our CDM-8 model.

Due to uncertainties in the physics of star formation, it is currently not possible to put strong constraints on DMF models using the 21-cm absorption line. We expect that future studies will be able to provide answers to the above open questions, providing a better understanding of the star formation physics at the redshifts involved in the 21-cm global absorption profile.

We conclude commenting on how our results will change when considering larger or lower values of M_{min} than those considered here for CDM. A larger value for M_{min} than $10^8 h^{-1} M_\odot$ makes the 21-cm absorption signal set-in more suddenly, because of the more rapid increase in the number density of such halos around $z \sim 17$, compared to the case of CDM-8. However, that also means that the star forming halos are rarer, and hence this requires a larger value of f_* in order to produce enough Lyman- α photons by $z \sim 17$, even larger than the $\sim 1.7\%$ of the CDM-8 model. Such

high values of f_* are unlikely, both on theoretical grounds, and based on the observed low M_*/M_h fractions of present-day low-mass galaxies. Much *lower* values of f_* are possible when lowering M_{\min} to values $< 10^7 h^{-1} M_\odot$. However, as commented above, this makes the onset of the 21-cm signal too shallow (much more shallower than that in CDM-7), and is also more in tension with the onset of *reionization* than CDM-7.

Acknowledgments

We thank Sownak Bose, Michael Buehlmann, Marius Cautun, Liang Gao, Oliver Hahn, John Regan and John Wise for valuable discussions. We also thank an anonymous referee for a very careful reading of the paper and their numerous comments that improved the manuscript. We are grateful to Alexey Boyarsky and Oleg Ruchayskiy for sharing their work [87] and for their comments on this manuscript. We thank John Helly for providing us with the software to identify collapsed regions, Jordan Mirocha for his help with ARES, Mark Lovell, Arvind Kumar Mishra and Guochao Sun for their comments on the manuscript. ML and BL are supported by the European Research Council via grant ERC-StG-716532-PUNCA. BL is additionally supported by STFC Consolidated Grants ST/P000541/1, ST/L00075X/1. SP is supported by the European Research Council under ERC Grant ‘‘NuMass’’ (FP7- IDEAS-ERC ERC-CG 617143) and acknowledges partial support from the Wolfson Foundation and the Royal Society. SP, CMB and BL are also supported in part by the European Union’s Horizon 2020 research and innovation program under the Marie Skłodowska-Curie grant agreements No. 690575 (RISE InvisiblesPlus) and 674896 (ITN Elusives). This work used the DiRAC@Durham facility managed by the Institute for Computational Cosmology on behalf of the STFC DiRAC HPC Facility (www.dirac.ac.uk). The equipment was funded by BEIS capital funding via STFC capital grants ST/K00042X/1, ST/P002293/1, ST/R002371/1 and ST/S002502/1, Durham University and STFC operations grant ST/R000832/1. DiRAC is part of the National e-Infrastructure.

A Reionization

Here, we address the reionization process in CDM-7 and CDM-8. To do so, we estimate the cumulative number density of ionizing photons with energy between [13.6, 24.6] eV produced at a given redshift as,

$$n_\gamma^{\text{ion}}(z) = \int_z^\infty dz' \frac{dn_\gamma^{\text{ion}}(z')}{dz'}, \quad (\text{A.1})$$

where $dn_\gamma^{\text{ion}}/dz$ is the number density of ionizing photons produced in the time interval corresponding to dz (the number of ionizing photons is calculated using ARES as in [115, 121]). $dn_\gamma^{\text{ion}}/dz$ can be given in terms of the ionization rate [121],

$$\Gamma_{\text{HI}} = N_{\text{ion}} f_{\text{esc}} \dot{\rho}_* \quad (\text{A.2})$$

which depends on the star formation rate density, $\dot{\rho}_*$ (note that $\dot{\rho}_*$ depends on f_* , see Eq. (2.15)) and on the fraction of ionizing photons (per stellar baryon) that can escape from their host galaxies, $f_{\text{esc}} N_{\text{ion}}$, where N_{ion} is the number of ionizing photons emitted per stellar baryon. Here, we consider $N_{\text{ion}} = 4000$ [7]. We approximately estimate the redshift of reionization, z_{ion} , as the redshift by which, cumulatively, two ionizing photons per baryon were emitted, $x_{\text{ion}} = 2$ ($x_{\text{ion}} \equiv n_\gamma^{\text{ion}}/n_b$ and n_b is the number density of baryons). Since x_{ion} depends on $f_* f_{\text{esc}}$, taking f_* from Table 2, we can estimate for each model the escape fraction needed to achieve $x_{\text{ion}} = 2$. This result is shown in Figure 3. Since $f_{\text{esc}} \leq 1$ by definition, from Figure 3 we conclude that a value of $f_* = 0.003$

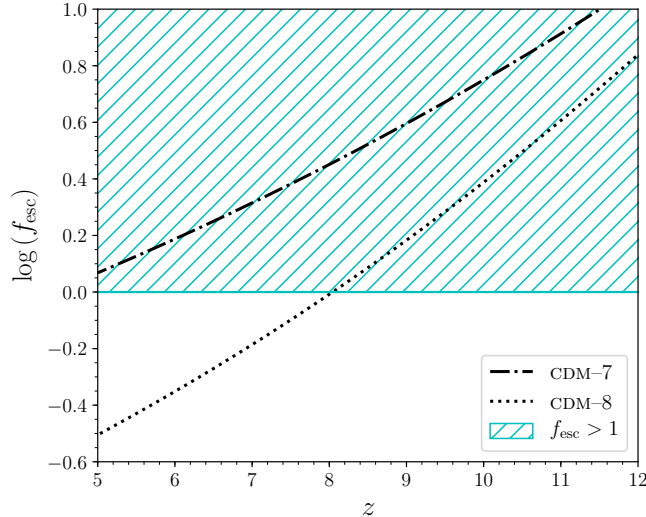


Figure 3. Escape fraction of ionizing photons, f_{esc} , needed to achieve $x_{\text{ion}} = 2$ at a given redshift, for the two CDM models CDM-7 and CDM-8 (as labelled). The shaded area shows the region where $f_{\text{esc}} > 1$. Since $f_{\text{esc}} \leq 1$ by definition, this region is not allowed.

(that produces an absorption trough in line with the timing of the EDGES signal, see Section 2.3) for CDM-7 cannot ensure reionization at redshifts $z > 5$. On the other hand, $f_{\text{esc}} \leq 1$ at $z \leq 8$ in the case of CDM-8, in better agreement with the evidence of reionization at $z \approx 7$.

References

- [1] P. J. E. Peebles, *Recombination of the Primeval Plasma*, *Astrophys. J.* **153**, 1, 1968.
- [2] S. A. Wouthuysen, *On the excitation mechanism of the 21-cm (radio-frequency) interstellar hydrogen emission line*, *AJ* **57**, 31 (1952).
- [3] G. B. Field, *Excitation of the Hydrogen 21-CM Line*, *Proceedings of the IRE* **46**, 240 (1958).
- [4] P. Tozzi, P. Madau, A. Meiksin and M. J. Rees, *Radio signatures of hi at high redshift: mapping the end of the “dark ages”*, *Astrophys. J.* **528**, 597 (2000) [astro-ph/9903139].
- [5] X. L. Chen and J. Miralda-Escude, *The spin - kinetic temperature coupling and the heating rate due to Lyman - alpha scattering before reionization: Predictions for 21cm emission and absorption*, *Astrophys. J.* **602**, 1 (2004) [astro-ph/0303395].
- [6] M. Ricotti, J. P. Ostriker and N. Y. Gnedin, *X-ray preionization powered by accretion on the first black holes. 2: Cosmological simulations and observational signatures*, *Mon. Not. Roy. Astron. Soc.* **357**, 207 (2005) [astro-ph/0404318].
- [7] R. Barkana and A. Loeb, *In the beginning: The First sources of light and the reionization of the Universe*, *Phys. Rept.* **349**, 125 (2001) [astro-ph/0010468].
- [8] S. Furlanetto, *The Global 21 Centimeter Background from High Redshifts*, *Mon. Not. Roy. Astron. Soc.* **371**, 867 (2006) [astro-ph/0604040].
- [9] S. Furlanetto, S. P. Oh and F. Briggs, *Cosmology at Low Frequencies: The 21 cm Transition and the High-Redshift Universe*, *Phys. Rept.* **433**, 181 (2006) [astro-ph/0608032].
- [10] J. R. Pritchard and A. Loeb, *21 cm cosmology in the 21st century*, *Rept. Prog. Phys.* **75**, 086901 (2012) [arXiv:1109.6012 [astro-ph.CO]].

- [11] A. Lewis and A. Challinor, *The 21cm angular-power spectrum from the dark ages*, Phys. Rev. D **76**, 083005 (2007) [astro-ph/0702600 [ASTRO-PH]].
- [12] J. O. Burns, *et al.*, Astrophys. J., **844**, 33 (2017) [arXiv:1704.02651 [astro-ph.IM]].
- [13] J. D. Bowman, A. E. E. Rogers, R. A. Monsalve, T. J. Mozdzen and N. Mahesh, *An absorption profile centred at 78 megahertz in the sky-averaged spectrum*, Nature **555**, 67 (2018).
- [14] R. Barkana, *Possible interaction between baryons and dark-matter particles revealed by the first stars*, Nature **555**, no. 7694, 71 (2018) [arXiv:1803.06698 [astro-ph.CO]].
- [15] C. Feng and G. Holder, *Enhanced global signal of neutral hydrogen due to excess radiation at cosmic dawn*, Astrophys. J. **858**, no. 2, L17 (2018) [arXiv:1802.07432 [astro-ph.CO]].
- [16] J. B. Munoz and A. Loeb, *A small amount of mini-charged dark matter could cool the baryons in the early Universe*, Nature **557**, no. 7707, 684 (2018) [arXiv:1802.10094 [astro-ph.CO]].
- [17] A. Berlin, D. Hooper, G. Krnjaic and S. D. McDermott, *Severely Constraining Dark Matter Interpretations of the 21-cm Anomaly*, Phys. Rev. Lett. **121**, no. 1, 011102 (2018) [arXiv:1803.02804 [hep-ph]].
- [18] R. Barkana, N. J. Outmezguine, D. Redigolo and T. Volansky, *Signs of Dark Matter at 21-cm?*, Phys. Rev. D **98**, no. 10, 103005 (2018) [arXiv:1803.03091 [hep-ph]].
- [19] S. Fraser *et al.*, *The EDGES 21 cm Anomaly and Properties of Dark Matter*, Phys. Lett. B **785**, 159 (2018) [arXiv:1803.03245 [hep-ph]].
- [20] T. R. Slatyer and C. L. Wu, *Early-Universe constraints on dark matter-baryon scattering and their implications for a global 21 cm signal*, Phys. Rev. D **98**, no. 2, 023013 (2018) [arXiv:1803.09734 [astro-ph.CO]].
- [21] P. Sharma, *Astrophysical radio background cannot explain the EDGES 21-cm signal: constraints from cooling of non-thermal electrons*, Mon. Not. Roy. Astron. Soc. **481**, no. 1, L6 (2018) [arXiv:1804.05843 [astro-ph.HE]].
- [22] P. Sikivie, *Axion dark matter and the 21-cm signal*, Phys. Dark Univ. , 100289 [arXiv:1805.05577 [astro-ph.CO]].
- [23] N. Houston, C. Li, T. Li, Q. Yang and X. Zhang, *Natural Explanation for 21 cm Absorption Signals via Axion-Induced Cooling*, Phys. Rev. Lett. **121**, no. 11, 111301 (2018) [arXiv:1805.04426 [hep-ph]].
- [24] C. Li and Y. F. Cai, *Searching for the Dark Force with 21-cm Spectrum in Light of EDGES*, Phys. Lett. B **788**, 70 (2019) [arXiv:1804.04816 [astro-ph.CO]].
- [25] L. B. Jia, *Dark photon portal dark matter with the 21-cm anomaly*, Eur. Phys. J. C **79**, no. 1, 80 (2019) [arXiv:1804.07934 [hep-ph]].
- [26] J. R. Bhatt, A. K. Mishra and A. C. Nayak, *Viscous dark matter and 21 cm cosmology*, (2019) [arXiv:1901.08451 [astro-ph.CO]].
- [27] A. Chatterjee, P. Dayal, T. R. Choudhury and A. Hutter, *Ruling out 3 keV warm dark matter using 21 cm-EDGES data*, arXiv:1902.09562 [astro-ph.CO].
- [28] A. K. Mishra, *Lightening the Dark Matter from its Viscosity and Explanation of EDGES Anomaly*, (2019) [arXiv:1907.04238 [astro-ph.CO]].
- [29] M. Spinelli, G. Bernardi and M. G. Santos, *On the contamination of the global 21 cm signal from polarized foregrounds*, (2019) [arXiv:1908.05303 [astro-ph.CO]].
- [30] R. Hills, G. Kulkarni, P. D. Meerburg and E. Puchwein, *Concerns about modelling of the EDGES data*, Nature **564**, no. 7736, E32 (2018) [arXiv:1805.01421 [astro-ph.CO]].
- [31] J. D. Bowman, A. E. E. Rogers, R. A. Monsalve, *et al.*, *Reply to Hills et al.*, Nature **564**, E35 (2018).
- [32] S. Singh and R. Subrahmanyam, *The redshifted 21-cm signal in the EDGES low-band spectrum*, [arXiv:1903.04540 [astro-ph.CO]].

- [33] G. D’Amico, P. Panci and A. Strumia, *Bounds on Dark Matter annihilations from 21 cm data*, Phys. Rev. Lett. **121**, no. 1, 011103 (2018) [arXiv:1803.03629 [astro-ph.CO]].
- [34] J. C. Hill and E. J. Baxter, *Can Early Dark Energy Explain EDGES?*, JCAP **1808**, no. 08, 037 (2018) [arXiv:1803.07555 [astro-ph.CO]].
- [35] A. Hektor, G. Hutsi, L. Marzola, M. Raidal, V. Vaskonen and H. Veermae, *Constraining Primordial Black Holes with the EDGES 21-cm Absorption Signal*, Phys. Rev. D **98**, no. 2, 023503 (2018) [arXiv:1803.09697 [astro-ph.CO]].
- [36] A. Mitridate and A. Podo, *Bounds on Dark Matter decay from 21 cm line*, JCAP **1805**, no. 05, 069 (2018) [arXiv:1803.11169 [hep-ph]].
- [37] Y. Wang and G. B. Zhao, *Constraining the dark matter-vacuum energy interaction using the EDGES 21-cm absorption signal*, Astrophys. J. **869**, no. 1, 26 (2018) [arXiv:1805.11210 [astro-ph.CO]].
- [38] C. Li, X. Ren, M. Khurshudyan and Y. F. Cai, *Implications of the possible 21-cm line excess at cosmic dawn on dynamics of interacting dark energy*, [arXiv:1904.02458 [astro-ph.CO]].
- [39] W. Yang, S. Pan, S. Vagnozzi, E. Di Valentino, D. F. Mota and S. Capozziello, *Dawn of the dark: unified dark sectors and the EDGES Cosmic Dawn 21-cm signal*, [arXiv:1907.05344 [astro-ph.CO]].
- [40] T. Abel, G. L. Bryan and M. L. Norman, *The formation of the first star in the Universe*, Science **295**, 93 (2002) [astro-ph/0112088].
- [41] H. Susa, K. Hasegawa and N. Tominaga, *The Mass Spectrum of the First Stars*, Astrophys. J. **792**, no. 1, 32 (2014) [arXiv:1407.1374 [astro-ph.GA]].
- [42] S. Hirano, T. Hosokawa, N. Yoshida, K. Omukai and H. W. Yorke, *Primordial star formation under the influence of far ultraviolet radiation: 1540 cosmological haloes and the stellar mass distribution*, Mon. Not. Roy. Astron. Soc. **448**, no. 1, 568 (2015) [arXiv:1501.01630 [astro-ph.GA]].
- [43] A. Stacy, V. Bromm and A. T. Lee, *Building up the Population III initial mass function from cosmological initial conditions*, Mon. Not. Roy. Astron. Soc. **462**, 1307, [arXiv:1603.09475 [astro-ph.GA]].
- [44] D. Schaerer, *On the Properties of massive population III stars and metal-free stellar populations*, Astron. Astrophys. **382**, 28 (2002) [astro-ph/0110697].
- [45] J. Mirocha and S. R. Furlanetto, *What does the first highly-redshifted 21-cm detection tell us about early galaxies?*, Mon. Not. Roy. Astron. Soc. **483**, no. 2, 1980 (2019) [arXiv:1803.03272 [astro-ph.GA]].
- [46] A. A. Kaurov, T. Venumadhav, L. Dai and M. Zaldarriaga, *Implication of the Shape of the EDGES Signal for the 21 cm Power Spectrum*, Astrophys. J. **864**, no. 1, L15 (2018) [arXiv:1805.03254 [astro-ph.CO]].
- [47] P. Bode, J. P. Ostriker, N. Turok, *Halo formation in warm dark matter models*, Astrophys. J. **556**, 93-107 (2001) [arXiv:astro-ph/0010389].
- [48] P. Colin, V. Avila-Reese, O. Valenzuela, *Substructure and halo density profiles in a warm dark matter cosmology*, Astrophys. J. **542**, 622-630 (2000) [arXiv:astro-ph/0004115].
- [49] S. H. Hansen, J. Lesgourgues, S. Pastor, J. Silk, *Constraining the window on sterile neutrinos as warm dark matter*, Mon. Not. Roy. Astron. Soc. **333**, 544-546 (2002) [arXiv:astro-ph/0106108].
- [50] M. Viel, J. Lesgourgues, M. G. Haehnelt, S. Matarrese, A. Riotto, *Constraining warm dark matter candidates including sterile neutrinos and light gravitinos with WMAP and the Lyman-alpha forest*, Phys. Rev. D **71**, 063534 (2005) [arXiv:astro-ph/0501562].
- [51] S. Dodelson, L. M. Widrow, *Sterile-neutrinos as dark matter*, Phys. Rev. Lett. **72**, 17-20 (1994) [arXiv:hep-ph/9303287].
- [52] A. D. Dolgov, S. H. Hansen, *Massive sterile neutrinos as warm dark matter*, Astropart. Phys. **16**, 339-344 (2002) [arXiv:hep-ph/0009083].

- [53] T. Asaka, M. Laine, M. Shaposhnikov, *Lightest sterile neutrino abundance within the nuMSM*, JHEP **01**, 091 (2007) [Erratum: JHEP02,028(2015)] [arXiv:hep-ph/0612182].
- [54] K. Enqvist, K. Kainulainen, J. Maalampi, *Resonant neutrino transitions and nucleosynthesis*, Phys. Lett. B **249**, 531-534 (1990).
- [55] X. Shi, G. M. Fuller, *A New dark matter candidate: Nonthermal sterile neutrinos*, Phys. Rev. Lett. **82**, 2832 (1999) [arXiv:astro-ph/9810076].
- [56] K. Abazajian, G. M. Fuller, M. Patel, *Sterile neutrino hot, warm, and cold dark matter*, Phys. Rev. D **64**, 023501 (2001) [arXiv:astro-ph/0101524].
- [57] A. Kusenko, *Sterile neutrinos, dark matter, and the pulsar velocities in models with a Higgs singlet*, Phys. Rev. Lett. **97**, 241301 (2006) [arXiv:hep-ph/0609081].
- [58] K. Petraki, A. Kusenko, *Dark-matter sterile neutrinos in models with a gauge singlet in the Higgs sector*, Phys. Rev. D **77**, 065014 (2008) [arXiv:0711.4646 [hep-ph]].
- [59] A. Merle, M. Totzauer, *keV Sterile Neutrino Dark Matter from Singlet Scalar Decays: Basic Concepts and Subtle Features*, JCAP **1506**, 011 (2015) [arXiv:1502.01011 [hep-ph]].
- [60] J. König, A. Merle, M. Totzauer, *keV Sterile Neutrino Dark Matter from Singlet Scalar Decays: The Most General Case*, JCAP **1611**, 038 (2016) [arXiv:1609.01289 [hep-ph]].
- [61] D. N. Spergel, P. J. Steinhardt, *Observational evidence for selfinteracting cold dark matter*, Phys. Rev. Lett. **84**, 3760-3763 (2000) [arXiv:astro-ph/9909386].
- [62] C. Boehm, R. Schaeffer, *Constraints on dark matter interactions from structure formation: Damping lengths*, Astron. Astrophys. **438**, 419-442 (2005) [arXiv:astro-ph/0410591].
- [63] C. Boehm, J. A. Schewtschenko, R. J. Wilkinson, C. M. Baugh, S. Pascoli, *Using the Milky Way satellites to study interactions between cold dark matter and radiation*, Mon. Not. Roy. Astron. Soc. **445**, L31-L35 (2014) [arXiv:1404.7012 [astro-ph.CO]].
- [64] D. J. E. Marsh, *Axion Cosmology*, Phys. Rept. **643**, 1 (2016) [arXiv:1510.07633 [astro-ph.CO]].
- [65] J. Veltmaat, J. C. Niemeyer, *Cosmological particle-in-cell simulations with ultralight axion dark matter*, Phys. Rev. D **94**, no. 12, 123523 (2016) [arXiv:1608.00802 [astro-ph.CO]].
- [66] J. Veltmaat, J. C. Niemeyer and B. Schwabe, *Formation and structure of ultralight bosonic dark matter halos*, Phys. Rev. D **98**, no. 4, 043509 (2018) [arXiv:1804.09647 [astro-ph.CO]].
- [67] M. Kamionkowski and A. R. Liddle, *The Dearth of halo dwarf galaxies: Is there power on short scales?*, Phys. Rev. Lett. **84**, 4525 (2000) [astro-ph/9911103].
- [68] S. E. Hong, H. J. Lee, Y. J. Lee, E. D. Stewart and H. Zee, *Effects of thermal inflation on small scale density perturbations*, JCAP **1506**, 002 (2015) [arXiv:1503.08938 [astro-ph.CO]].
- [69] S. E. Hong, H. Zee and K. Ahn, *Small-scale Effects of Thermal Inflation on Halo Abundance at High- z , Galaxy Substructure Abundance and 21-cm Power Spectrum*, Phys. Rev. D **96**, no. 10, 103515 (2017) [arXiv:1706.08049 [astro-ph.CO]].
- [70] M. Leo, C. M. Baugh, B. Li and S. Pascoli, *N-body simulations of structure formation in thermal inflation cosmologies*, JCAP **1812**, no. 12, 010 (2018) [arXiv:1807.04980 [astro-ph.CO]].
- [71] K. Enqvist, T. Sawala and T. Takahashi, *Structure Formation with Two Periods of Inflation: Beyond $PLaIn \Lambda$ CDM*, [arXiv:1905.13580 [astro-ph.CO]].
- [72] L. Gao and T. Theuns, *Lighting the Universe with filaments*, Science **317**, 1527 (2007) [arXiv:0709.2165 [astro-ph]].
- [73] S. Hirano, J. M. Sullivan and V. Bromm, *First star formation in ultralight particle dark matter cosmology*, Mon. Not. Roy. Astron. Soc. **473**, no. 1, L6 (2018) [arXiv:1706.00435 [astro-ph.CO]].
- [74] M. Shaposhnikov, *A Possible symmetry of the nuMSM*, Nucl. Phys. B **763**, 49 (2007) [hep-ph/0605047].

- [75] A. Boyarsky, M. Drewes, T. Lasserre, S. Mertens and O. Ruchayskiy, *Sterile Neutrino Dark Matter*, Prog. Part. Nucl. Phys. **104**, 1 (2019) [arXiv:1807.07938 [hep-ph]].
- [76] D. H. Weinberg, J. S. Bullock, F. Governato, R. Kuzio de Naray and A. H. G. Peter, *Cold dark matter: controversies on small scales*, Proc. Nat. Acad. Sci. **112**, 12249 (2015) [arXiv:1306.0913 [astro-ph.CO]].
- [77] A. Garzilli, A. Boyarsky and O. Ruchayskiy, *Cutoff in the Lyman α forest power spectrum: warm IGM or warm dark matter?*, Phys. Lett. B **773**, 258 (2017) [arXiv:1510.07006 [astro-ph.CO]].
- [78] V. Irsic *et al.*, *New Constraints on the free-streaming of warm dark matter from intermediate and small scale Lyman- α forest data*, Phys. Rev. D **96**, no. 2, 023522 (2017) [arXiv:1702.01764 [astro-ph.CO]].
- [79] R. Murgia, A. Merle, M. Viel, M. Totzauer and A. Schneider, *“Non-cold” dark matter at small scales: a general approach*, JCAP **1711**, 046 (2017) [arXiv:1704.07838 [astro-ph.CO]].
- [80] A. Garzilli, A. Magalich, T. Theuns, C. S. Frenk, C. Weniger, O. Ruchayskiy and A. Boyarsky, *The Lyman- α forest as a diagnostic of the nature of the dark matter*, [arXiv:1809.06585 [astro-ph.CO]].
- [81] M. R. Lovell, C. S. Frenk, V. R. Eke, A. Jenkins, L. Gao and T. Theuns, *The properties of warm dark matter haloes*, Mon. Not. Roy. Astron. Soc. **439**, 300 (2014) [arXiv:1308.1399 [astro-ph.CO]].
- [82] M. R. Lovell, S. Bose, A. Boyarsky, et al., Mon. Not. Roy. Astron. Soc. **468**, 4285 (2017) [arXiv:1611.00010 [astro-ph.GA]].
- [83] A. Schneider, *Constraining noncold dark matter models with the global 21-cm signal*, Phys. Rev. D **98**, no. 6, 063021 (2018) [arXiv:1805.00021 [astro-ph.CO]].
- [84] A. Lidz and L. Hui, *Implications of a preionization 21-cm absorption signal for fuzzy dark matter*, Phys. Rev. D **98**, no. 2, 023011 (2018) [arXiv:1805.01253 [astro-ph.CO]].
- [85] M. Safarzadeh, E. Scannapieco and A. Babul, *A limit on the warm dark matter particle mass from the redshifted 21 cm absorption line*, Astrophys. J. **859**, no. 2, L18 (2018) [arXiv:1803.08039 [astro-ph.CO]].
- [86] L. Lopez-Honorez, O. Mena and P. Villanueva-Domingo, *Dark matter microphysics and 21 cm observations*, Phys. Rev. D **99**, no. 2, 023522 (2019) [arXiv:1811.02716 [astro-ph.CO]].
- [87] A. Boyarsky, D. Iakubovskyi, O. Ruchayskiy, A. Rudakovskiy and W. Valkenburg, *21-cm observations and warm dark matter models*, arXiv:1904.03097 [astro-ph.CO].
- [88] R. Barkana and A. Loeb, *Detecting the earliest galaxies through two new sources of 21cm fluctuations*, Astrophys. J. **626**, 1 (2005) [astro-ph/0410129].
- [89] J. R. Pritchard and S. R. Furlanetto, *Descending from on high: lyman series cascades and spin-kinetic temperature coupling in the 21 cm line*, Mon. Not. Roy. Astron. Soc. **367**, 1057 (2006) [astro-ph/0508381].
- [90] C. M. Hirata, *Wouthuysen-Field coupling strength and application to high-redshift 21 cm radiation*, Mon. Not. Roy. Astron. Soc. **367**, 259 (2006) [astro-ph/0507102].
- [91] B. Ciardi and P. Madau, *Probing beyond the epoch of hydrogen reionization with 21 centimeter radiation*, Astrophys. J. **596**, 1 (2003) doi:10.1086/377634 [astro-ph/0303249].
- [92] R. K. Sheth, G. Tormen, *Large scale bias and the peak background split*, Mon. Not. Roy. Astron. Soc. **308**, 119 (1999) [arXiv:astro-ph/9901122].
- [93] W. H. Press, P. Schechter, *Formation of galaxies and clusters of galaxies by selfsimilar gravitational condensation*, Astrophys. J. **187**, 425 (1974).
- [94] J. R. Bond, S. Cole, G. Efstathiou, N. Kaiser, *Excursion set mass functions for hierarchical Gaussian fluctuations*, Astrophys. J. **379**, 440 (1991).
- [95] A. R. Zentner, *The Excursion Set Theory of Halo Mass Functions, Halo Clustering, and Halo Growth*, Int. J. Mod. Phys. D **16**, 763 (2007) [arXiv:astro-ph/0611454].

- [96] A. J. Benson, A. Farahi, S. Cole, L. A. Moustakas, A. Jenkins, M. Lovell, R. Kennedy, J. Helly, C. Frenk, *Dark matter halo merger histories beyond cold dark matter - I. Methods and application to warm dark matter*, MNRAS **428**, 1774B (2013) [arXiv:1209.3018 [astro-ph.CO]].
- [97] A. Schneider, R. E. Smith and D. Reed, *Halo Mass Function and the Free Streaming Scale*, Mon. Not. Roy. Astron. Soc. **433**, 1573 (2013) [arXiv:1303.0839 [astro-ph.CO]].
- [98] A. Schneider, *Structure formation with suppressed small-scale perturbations*, Mon. Not. Roy. Astron. Soc. **451**, no. 3, 3117 (2015) [arXiv:1412.2133 [astro-ph.CO]].
- [99] M. Leo, C. M. Baugh, B. Li and S. Pascoli, *A new smooth- k space filter approach to calculate halo abundances*, JCAP **1804**, no. 04, 010 (2018) [arXiv:1801.02547 [astro-ph.CO]].
- [100] J. Lesgourgues, *The Cosmic Linear Anisotropy Solving System (CLASS) I: Overview*, [arXiv:1104.2932 [astro-ph.IM]].
- [101] J. Lesgourgues, T. Tram, *The Cosmic Linear Anisotropy Solving System (CLASS) IV: efficient implementation of non-cold relics*, JCAP **09**, 032 (2011) [arXiv:1104.2935].
- [102] V. Springel, *The Cosmological simulation code GADGET-2*, Mon. Not. Roy. Astron. Soc. **364**, 1105 (2005) [astro-ph/0505010].
- [103] M. Crocce, S. Pueblas and R. Scoccimarro, *Transients from Initial Conditions in Cosmological Simulations*, Mon. Not. Roy. Astron. Soc. **373**, 369 (2006) [astro-ph/0606505].
- [104] R. E. Angulo, O. Hahn and T. Abel, *The Warm DM halo mass function below the cut-off scale*, Mon. Not. Roy. Astron. Soc. **434**, 3337 (2013) [arXiv:1304.2406 [astro-ph.CO]].
- [105] C. A. Correa, J. S. B. Wyithe, J. Schaye and A. R. Duffy, *The accretion history of dark matter haloes – I. The physical origin of the universal function*, Mon. Not. Roy. Astron. Soc. **450**, no. 2, 1514 (2015) [arXiv:1409.5228 [astro-ph.GA]].
- [106] D. Reed, R. Bower, C. Frenk, A. Jenkins and T. Theuns, *The halo mass function from the dark ages through the present day*, Mon. Not. Roy. Astron. Soc. **374**, 2 (2007) [astro-ph/0607150].
- [107] M. Sharma and T. Theuns, *The $I_{\kappa\epsilon\alpha}$ model of feedback-regulated galaxy formation*, (2019), [arXiv:1906.10135 [astro-ph.GA]].
- [108] T. Sawala *et al.*, *Bent by baryons: the low mass galaxy-halo relation*, Mon. Not. Roy. Astron. Soc. **448**, no. 3, 2941 (2015) [arXiv:1404.3724 [astro-ph.GA]].
- [109] C. Leitherer *et al.*, *Starburst99: Synthesis models for galaxies with active star formation*, Astrophys. J. Suppl. **123**, 3 (1999) [astro-ph/9902334].
- [110] G. Sun and S. R. Furlanetto, *Constraints on the star formation efficiency of galaxies during the epoch of reionization*, Mon. Not. Roy. Astron. Soc. **460**, 417 (2016) [arXiv:1512.06219 [astro-ph.GA]].
- [111] J. Mirocha, S. R. Furlanetto, G. Sun G., *The Global 21-cm Signal in the Context of the High- z Galaxy Luminosity Function*, Mon. Not. Roy. Astron. Soc. **464**, 1365 (2017) [arXiv:1607.00386 [astro-ph.GA]].
- [112] S. R. Furlanetto, J. Mirocha, R. H. Mebane, G. Sun, *A minimalist feedback-regulated model for galaxy formation during the epoch of reionization*, Mon. Not. Roy. Astron. Soc. **472**, 1576 (2017) [arXiv:1611.01169 [astro-ph.GA]].
- [113] M. L. Norman, P. Chen, J. H. Wise and H. Xu, *Fully Coupled Simulation of Cosmic Reionization. III. Stochastic Early Reionization by the Smallest Galaxies*, Astrophys. J. **867**, no. 1, 27 (2018) [arXiv:1705.00026 [astro-ph.CO]].
- [114] J. Mirocha, R. H. Mebane, S. R. Furlanetto, K. Singal and D. Trinh, *Unique signatures of Population III stars in the global 21-cm signal*, Mon. Not. Roy. Astron. Soc. **478**, no. 4, 5591 (2018) [arXiv:1710.02530 [astro-ph.GA]].
- [115] J. Mirocha, *Decoding the X-ray Properties of Pre-Reionization Era Sources*, Mon. Not. Roy. Astron. Soc. **443**, no. 2, 1211 (2014) [arXiv:1406.4120 [astro-ph.GA]].

- [116] J. Mirocha, S. Skory, J. O. Burns, J. H. Wise, *Optimized Multi-Frequency Spectra for Applications in Radiative Feedback and Cosmological Reionization*, *Astrophys. J.* **756**, 94 (2012) [arXiv:1204.1944 [astro-ph.CO]]
- [117] M. E. Machacek, G. L. Bryan and T. Abel, *Simulations of pregalactic structure formation with radiative feedback*, *Astrophys. J.* **548**, 509 (2001) [astro-ph/0007198].
- [118] D. Tseliakhovich and C. Hirata, *Relative velocity of dark matter and baryonic fluids and the formation of the first structures*, *Phys. Rev. D* **82**, 083520 (2010) [arXiv:1005.2416 [astro-ph.CO]].
- [119] M. L. A. Richardson, E. Scannapieco and R. J. Thacker, *Hybrid Cosmological Simulations with Stream Velocities*, *Astrophys. J.* **771**, 81 (2013) [arXiv:1305.3276 [astro-ph.CO]].
- [120] S. Naoz, N. Yoshida, N. Y. Gnedin, *Astrophys. J.* **763**, 27 (2013) [arXiv:1207.5515 [astro-ph.CO]]
- [121] J. Mirocha, G. J. A. Harker and J. O. Burns, *Interpreting the Global 21-cm Signal from High Redshifts. II. Parameter Estimation for Models of Galaxy Formation*, *Astrophys. J.* **813**, no. 1, 11 (2015) [arXiv:1509.07868 [astro-ph.CO]].